Delft University of Technology

Multispectral visual detection method for conveyor belt longitudinal tear

Hou, Chengcheng; Qiao, Tiezhu; Zhang, Haitao; Pang, Yusong; Xiong, Xiaoyan

Citation (APA)
Hou, C., Qiao, T., Zhang, H., Pang, Y., & Xiong, X. (2019). Multispectral visual detection method for conveyor belt longitudinal tear. *Measurement: Journal of the International Measurement Confederation*, *143*, 246-257. https://doi.org/10.1016/j.measurement.2019.05.010

Important note
To cite this publication, please use the final published version (if applicable).
Please check the document version above.

Multispectral visual detection method for
conveyor belt longitudinal tear

Chengcheng Hou [a], Tiezhu Qiao [a,*], Haitao Zhang [a], Yusong Pang [b]

[a] Key Laboratory of Advanced Transducers and Intelligent Control System, Ministry of Education, Taiyuan
University of Technology, Taiyuan 030024, China

[b] Section of Transport Engineering and Logistic, Faculty of Mechanical, Maritime and Materials Engineering,
Delft University of Technology, 2628 CD Delft, Netherlands

Abstract：As an important part of modern coal mine production, conveyor belts are widely used in the coal collection and transportation. In order to ensure the safe operation of coal mine conveyor belt and solve the drawbacks of the existing conveyor belt longitudinal tear detection technology, a multispectral visual detection method for conveyor belt longitudinal tear is proposed in this paper. The experimental results show that the multispectral visual detection method not only can identify the conveyor belt longitudinal tear, but also accurately classifies and identify other status of the conveyor belt. The accuracy rate of conveyor belt longitudinal tear detection is over 96.5%, and the average accuracy rate of all status of conveyor belt identification is over 96.1%. The proposed method is verified to meet the requirements of reliability and real-time in industrial field.

Keywords: Conveyor belt; Longitudinal tear; Multispectral visual detection; Image fusion

1. Introduction

Conveyor belt is an important transportation equipment in coal mine production process [1]. Once the conveyor belt longitudinal tear happened, it will cause huge economic loss and even human injury. Real-time and reliable conveyor belt longitudinal tear detection is essential [2][3]. There are many common longitudinal tear detection methods for conveyor belt at present [4], such as pre-fill coil detection method [5][6], contact detection method [7], leaking material detection method [8], etc. These detection methods are easily affected by the coal mine environment, resulting in reduced detection sensitivity or even equipment damage, and requiring frequent replacement of the detection equipment.

With the increasing in computer processing speed, machine vision technology has developed rapidly in recent years [9]. Compared with the traditional detection technology, machine vision detection technology has the advantages of high speed, high precision and non-contact long-term detection [10]. Therefore machine vision detection has become an important research in conveyor belt fault detection, and there are a variety of conveyor belt longitudinal tear detection methods based on machine vision technology [11-15]. Rosati et al. [12] proposed an automatic detection method

for coal conveyor belt surface crack by using the linear CCD(Charge Coupled Device) camera and light source. Li et al. [13] proposed a laser-based on-line machine vision detection method by using visible light CMOS(Complementary Metal Oxide Semiconductor) camera to capture the conveyor belt image, then analyzed to judge whether there is a rip on the belt surface or not. Yu et al. [14] proposed a dual band infrared detection method by using mid-infrared and long infrared vision. These detection methods used only visible light or infrared light. Although the visible light images can provide detailed target information and clear texture features, the underground environment of coal mine is harsh, and it is difficult for visible light camera to capture clear images. Infrared light detection method detects the conveyor belt longitudinal tear by using single-band infrared or dual-band infrared. However, due to the infrared imaging principle, the infrared image has problems of high noise, low contrast, poor visual effect, etc. Qiao et al. [15] proposed a longitudinal tear detection method based on visible light and infrared vision, the detection results cannot accurately determine the longitudinal tear category, especially wear and the wear or tear that has happened but have not repaired. Misidentification causes frequent emergency alarm and belt conveyor stop, which is damage to conveyor drive motor and conveyor belt. Therefore, it is necessary to design a new method to improve the accuracy of longitudinal tear detection and accurately distinguish normal, wear, wear or tear that has happened but have not repaired on conveyor belt, so as to avoid frequent wrong operation to belt conveyor.

Conveyor belts can be divided into ordinary conveyor belts and special structure conveyor belts. According to the material of cover layer and core layer, conveyor belts can be divided into rubber conveyor belts, plastic conveyor belts, nylon conveyor belts and steel cord conveyor belts [16][17].The structure of nylon conveyor belt and steel cord conveyor belt is shown in Fig.1. According to the research [14], the cover layer and core layer of conveyor belt made of different materials, their infrared radiation wavelengths are different. When the conveyor belt has cracks or scratches, the core layer will be exposed [18].At this time, we can use the mid-infrared CCD and the visible light CCD to capture surface image information of the conveyor belt, and the image information of cracks or scratches is different from other parts. Based on this property, the conveyor belt image can be captured by mid-infrared CCD and visible light CCD respectively, then fusing the mid-infrared and visible light images, and the cracks or scratches of the conveyor belt can be distinguished by analyzing the fused images.

In addition, the conveyor belt longitudinal tear generally occurs because the long bar iron or sheet gangue first rubs against the conveyor belt and then penetrates the conveyor belt [19]. When the conveyor belt is wearing, the temperature in the wearing zone rise and the wearing zone generate a lot of heat which radiate outward in the

form of far infrared. Therefore, the conveyor belt image can be captured by far infrared CCD and visible light CCD respectively, then fusing the far infrared and visible light images, and the conveyor belt wear can be judged by analyzing the fused images.
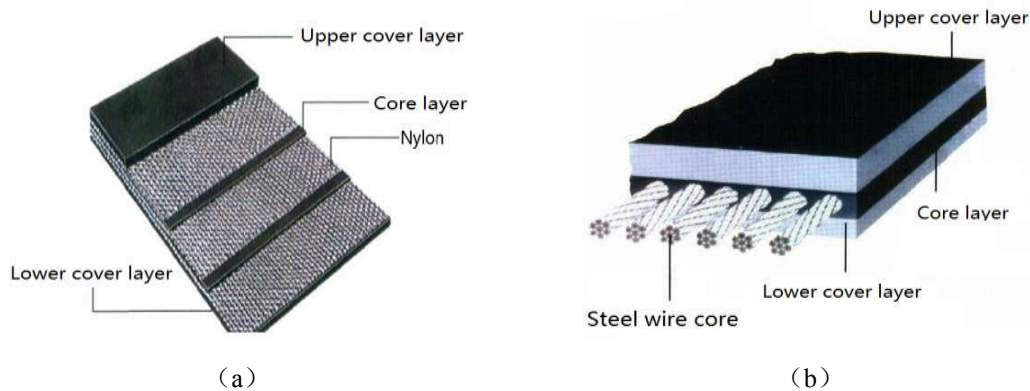

Fig.1.Structure of conveyor belt: (a) nylon conveyor belt; (b) steel cord conveyor belt

Based on the above analysis, combined with the operating environment of mining conveyor belts and the deficiencies of existing various longitudinal tear detection method, a multispectral visual detection method for conveyor belt longitudinal tear is proposed in this paper. The original light from conveyor belt is decomposed into visible light, mid-infrared light and far infrared light by using a dedicated multispectral image acquisition sensor. Then, according to the characteristics of conveyor belt longitudinal tear, the visible light image and mid-infrared images are fused, the visible light image and far infrared images are fused. Base on the results of dual fused images analysis, the status of conveyor belt can be divided into six situations: longitudinal tearing (longitudinal tear is happening), upper surface wearing (upper surface wear is happening), lower surface wearing (lower surface wear is happening), longitudinal tear has happened but have not repaired, wear has happened but have not repaired and conveyor belt normal. According to the analysis results, belt conveyor is set as normal running, warning alarm, danger alarm or stop operation respectively. The remainder of this paper is organized as follows. The Section 2 describes the multispectral visual detection method. Section 3 presents the experimental methods, results, and the analysis of experimental results. Finally, the conclusions of this paper are given in Section 4.

2. Multispectral visual detection method

The whole process of multispectral visual detection method for conveyor belt longitudinal tear is divided into five parts: image acquisition, image fusion, image processing, feature extraction and status analysis. In the image acquisition part, we use a new multispectral image acquisition sensor to complete the acquisition of visible light image, mid-infrared image and far infrared image. The image fusion part realizes

the fusion of visible and mid-infrared images and the fusion of visible and far infrared images. The image processing part mainly achieves image enhancement and image segmentation of fused images. The feature information of the conveyor belt status is extracted in the feature extraction part. In the status analysis part, the current status of conveyor belt is determined by combining the analysis results of the double fused images. The overall flowchart of multispectral visual detection method is shown in Fig.2.
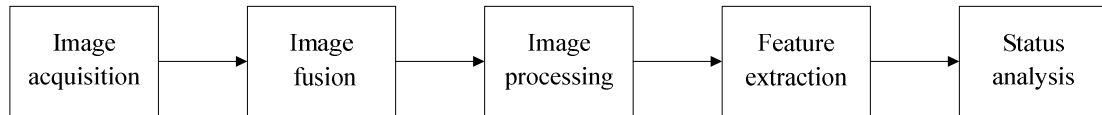
| Image acquisition | → | Image fusion | → | Image processing | → | Feature extraction | → | Status analysis |

Fig.2. Overall flowchart of multispectral visual detection method

2.1. Image acquisition

Image acquisition is the most important part in the whole multispectral visual detection method. A good image acquisition design not only can ensure the quality of images, but also can reduce the complexity of subsequent work. In this paper, a new multispectral image acquisition sensor is used for visible, mid-infrared and far infrared images acquisition [20].The schematic diagram of multispectral image acquisition sensor is shown in Fig.3.
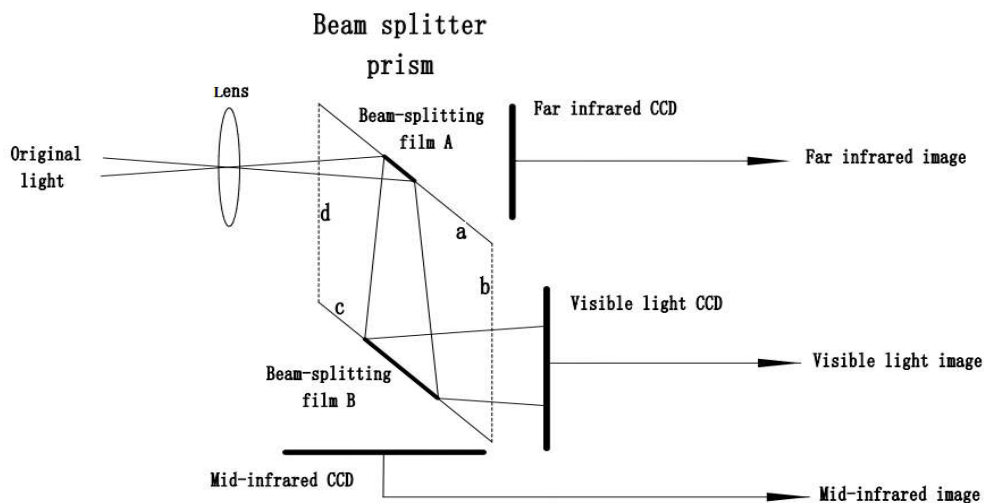

Fig.3. Schematic diagram of multispectral image acquisition sensor

The sensor mainly includes a lens, a diamond-shaped beam splitter prism, a far infrared CCD, a visible light CCD and a mid-infrared CCD. The 'a' side of beam splitter prism is plated with the beam-splitting film A (high transmittance for far infrared wavelength and high reflectance for visible light wavelength and mid-infrared wavelength), the 'c' side of beam splitter prism is plated with the beam-splitting film B (high transmittance for mid-infrared wavelength and high reflectance for visible light wavelength). The original light is focused into the beam splitter prism through the lens. The far infrared light in the original light enters into

the far-infrared CCD through the beam-splitting film A. The light of other wavelengths are reflected to 'c' side of the beam splitter prism. Then the mid-infrared light enters into the mid-infrared CCD through the beam-splitting film B, and the visible light is reflected into the visible light CCD. The original light is decomposed into visible light, mid-infrared light, and far infrared light by the beam splitter prism. Three kinds of CCD capture three types of light signal respectively, the visible light, mid-infrared light and far infrared light are converted to corresponding analog electric signal on the basis of photoelectric effect. After signal amplified, filtered and A/D converted processing, the visible light image, mid-infrared image and far infrared image of conveyor belt are finally obtained.

2.2. Image fusion

According to the characteristics of the conveyor belt longitudinal tear and wear, we need to make the visible light image and mid-infrared image pixel-level fused, and make the visible light image and far infrared image pixel-level fused. In the pixel-level fusion method [21][22], the method based on block fusion and region fusion becomes the focus of the research. Therefore, the image fusion rule based on discrete wavelet transform [23] and region feature [24] is adopted in this paper. Image fusion includes the following steps:

(1) The visible light image, mid-infrared image and far infrared image are respectively decomposed into low-frequency information (represent the approximate sub-image) and high-frequency information (represent the detail sub-image) by using discrete wavelet transform. High-frequency information is divided into a horizontal component, a vertical component and a diagonal component. The original image is represented by $f(x,y)$, using C_0, H and G to represent the one-dimensional wavelet filter matrix. The two-dimensional wavelet decomposition algorithm can be described as:

$$\begin{cases} C_{j+1} = HC_jH^{'} \\ D_{j+1}^{h} = GC_jH^{'} \\ D_{j+1}^{v} = HC_jG^{'} \\ D_{j+1}^{d} = GC_jG^{'} \end{cases} \quad (j=0,1,\cdots,J-1) \tag{1}$$

where h,v,d represent horizontal, vertical and diagonal component respectively, $H^{'}$ and $G^{'}$ are the conjugate transpose matrix of H and G respectively;

(2) The last decomposition layer of low-frequency information is merged by using the weighted average fusion rule. The calculation formula is as follows:

$$F(m,n)=\alpha*f_{1L}(m,n)+(1-\alpha)*f_{2L}(m,n) \tag{2}$$

where $f_{1L}(m,n)$ and $f_{2L}(m,n)$ are the low-frequency information of the original image $f_1(m,n)$ and $f_2(m,n)$, and $F(m,n)$ is the low-frequency information of

fusion image. α is the weight value, which is between 0-1. It is 0.5 in this paper;

(3) For the high-frequency information, the fusion rule based on the neighborhood average gradient is adopted, and the calculation formula is:

$$\bar{G} = \frac{1}{(M-1)*(N-1)}\sum_{i=1}^{M-1}\sum_{j=1}^{N-1}\sqrt{\frac{(D(i,j)-D(i+1,j))^2+(D(i,j)-D(i,j+1))^2}{2}} \qquad (3)$$

where $D(i,j)$ is the gray value of the row i and column j of the image, M and N are the total number of rows and the total number of columns of the image respectively;

(4) Image reconstruction. The visible and mid-infrared fused image (VMI image), and the visible and far infrared fused image (VFI image) can be obtained by using the inverse discrete wavelet transform. The transform algorithm is:

$$C_{j-1} = H'C_jH + G'D_j^hH + H'D_j^vG + G'D_j^dG \qquad (j=0,1,\cdots,J-1) \qquad (4)$$

Fig.4 shows the visible light image, mid-infrared image and VMI image about scratch. Fig.5 shows the visible light image, mid-infrared image and VMI image about crack. Fig.6 shows the visible light image, far infrared image and VFI image about wearing.
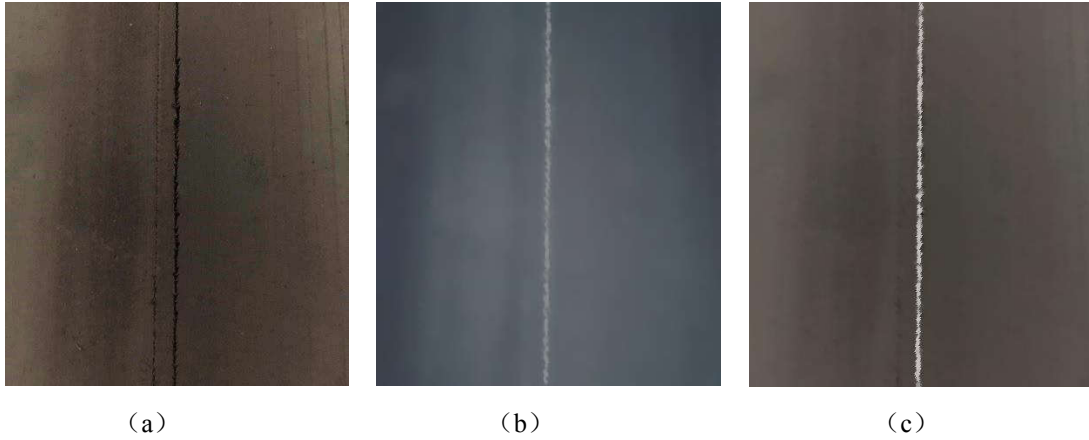

（a）　　　　　　　　　　（b）　　　　　　　　　　（c）

Fig.4. Scratch image: (a) visible light image; (b) mid-infrared image; (c) VMI image

（a）　　　　　　　　　　（b）　　　　　　　　　　（c）

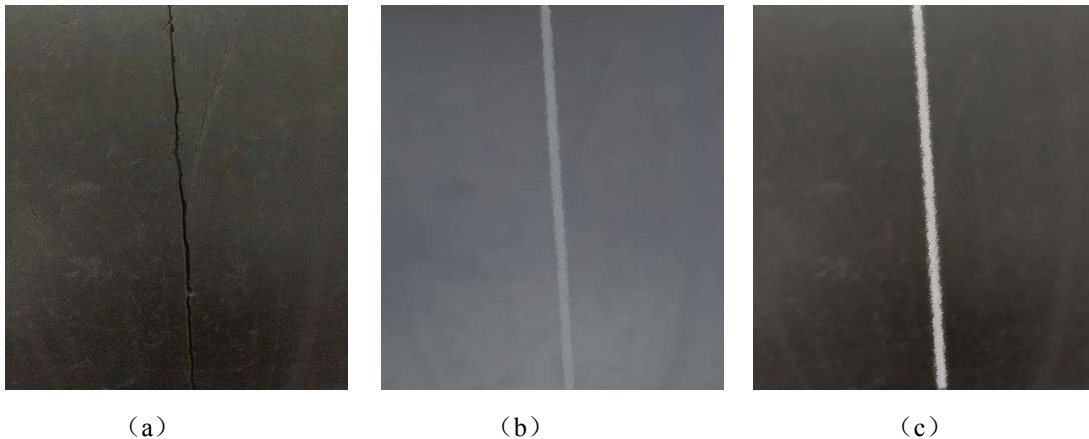**Fig.5.** Crack image: (a) visible light image; (b) mid-infrared image; (c) VMI image

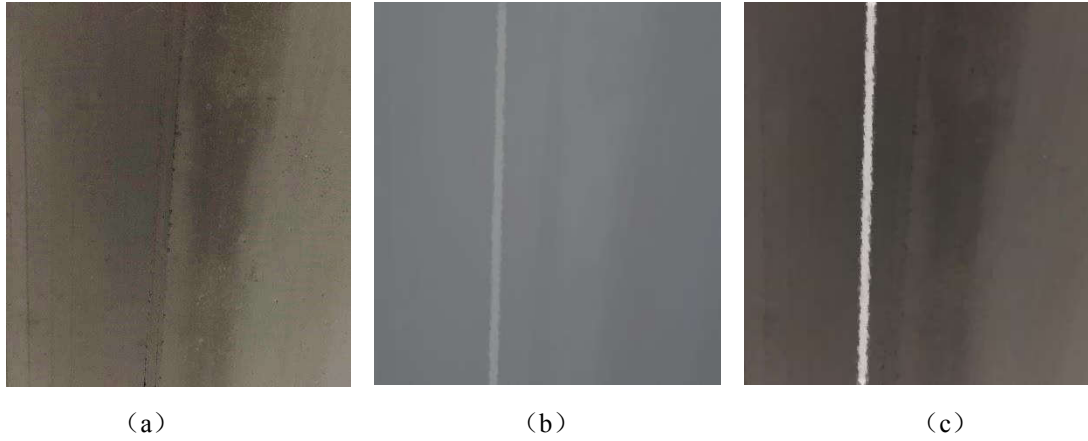(a)   (b)   (c)

Fig.6. Wearing image: (a) visible light image; (b) far infrared image; (c) VFI image

The process of image fusion algorithm based on discrete wavelet transform and region feature is shown in Fig.7.
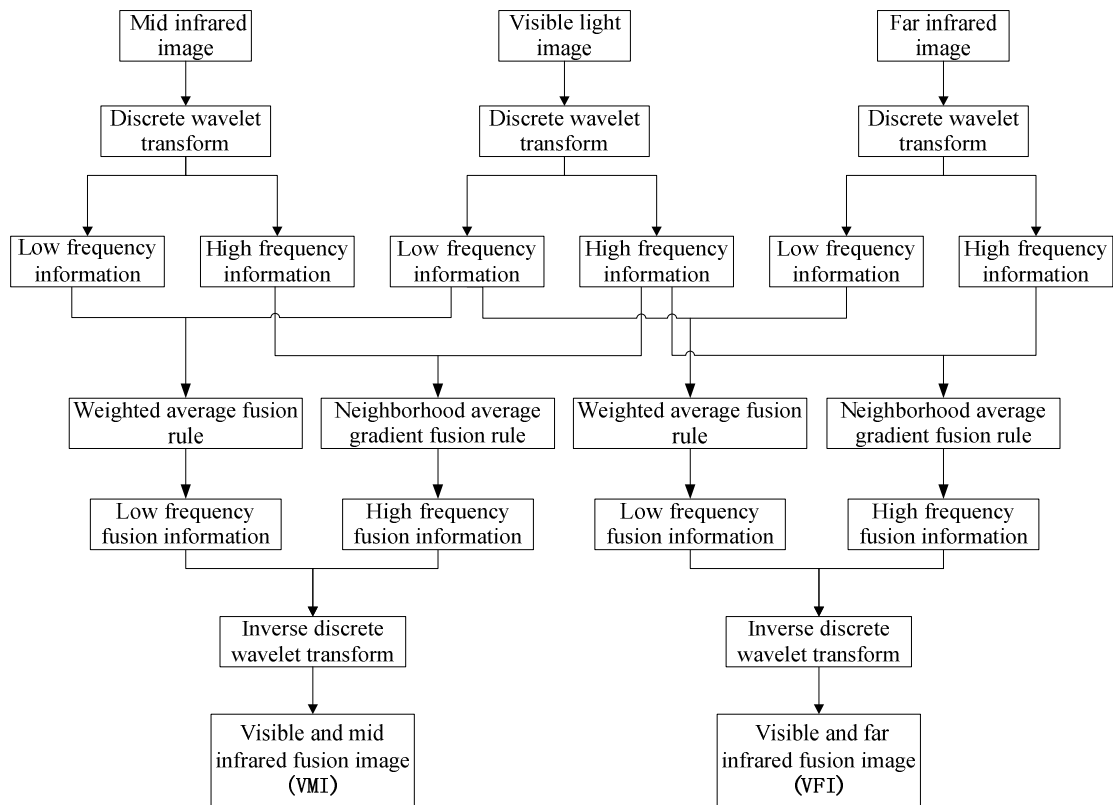
Fig.7. Block diagram of the image fusion process

2.3. Image processing

Dual-thread image processing is adopted in this paper for the VMI image and VFI image. First, the VMI image and the VFI image are median filtered to eliminate noise[25]. Then, image enhancement operation and image threshold segmentation are performed to obtain binary images of the VMI image and the VFI image.

2.3.1. Image enhancement

The tear or wear target in the conveyor belt image can be highlight by image

enhancement[26]. In this paper, histogram equalization[27] is used to improve the image quality, which make the gray histogram of original image change from a relatively concentrated grayscale range to a uniform distribution in the whole gray range. The histogram after equalization of crack image and wearing image are shown in Fig.8-(b) and Fig.9-(b) respectively. The steps of histogram equalization are as follows:

(1) List the gray levels of original image and transformed image: $i, j = 0,1,\cdots,L-1$, where L is the number of gray levels;

(2) Count the number of pixels N_i in each gray level of the original image;

(3) Calculate the histogram of original image:

$$P(i) = \frac{N_i}{N} \qquad (5)$$

where N is the total pixel value of the original image;

(4) Calculate the cumulative histogram:

$$P(j) = \sum_{k=0}^{j} P(k) \qquad (6)$$

(5) Calculate the transformed gray value by using the grayscale transformation function. The function is as follows:

$$j = INT[(L-1)*P(j)+0.5] \qquad (7)$$

where INT is the rounding function;

(6) Revise the gray value of the original image $f(m,n) = i$ to the gray value of transformed image $g(m,n) = j$;

(7) Count the number of pixels N_j in each gray level of transformed image;

(8) Calculate the histogram of the transformed image:
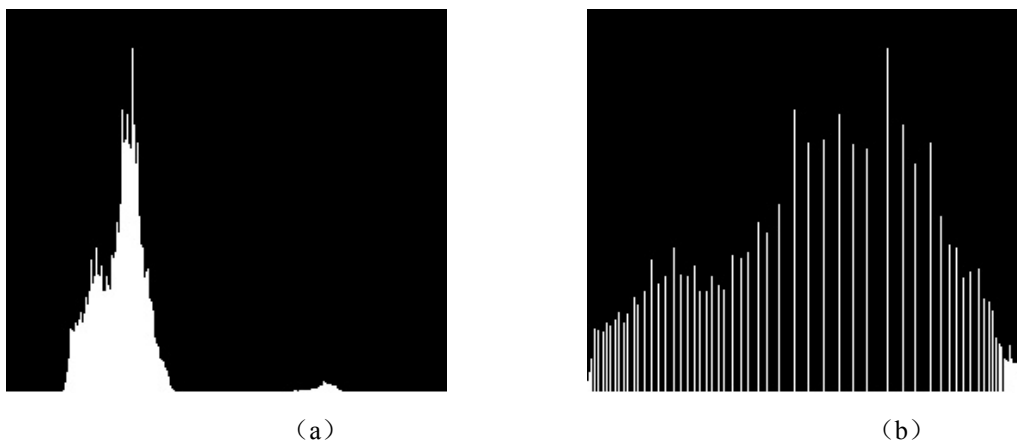
$$P(j) = \frac{N_j}{N} \qquad (8)$$

（a）   （b）

Fig.8. The histogram of crack image: (a) VMI image; (b) VMI image after equalization
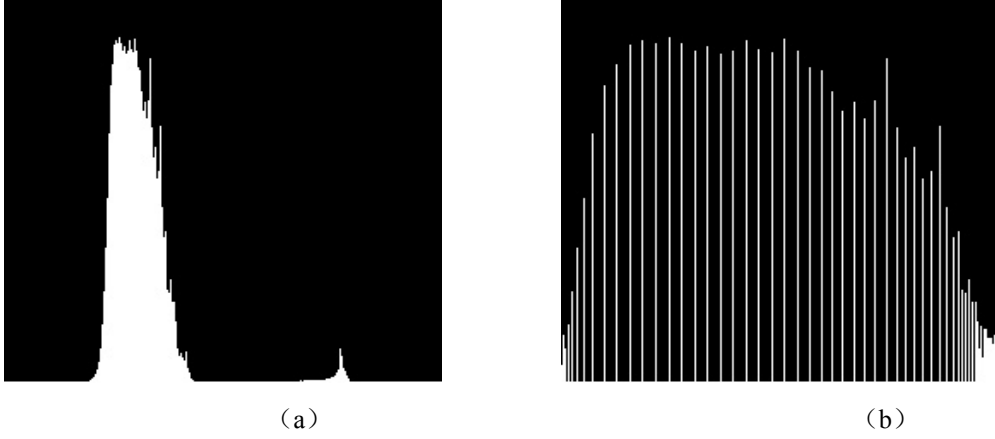
<center>（a）   （b）</center>

Fig.9. The histogram of wearing image: (a) VFI image; (b) VFI image after equalization

2.3.2. Threshold segmentation

After median filtering and image enhancement processing, the conveyor belt image is clearer and the target contour is more prominent. Local adaptive threshold segmentation algorithm [28] is used to extract the tear or wear profile information from VMI image and VFI image in this paper. The threshold value is calculated by using the maximum inter-class variance method. The specific algorithm principle is as follows:

Suppose the number of gray level of original image is L, N_i is the pixel number of gray level i in the original image, the total pixel value of the original image is $N = \sum_{i=0}^{L-1} N_i$, therefore the probability of gray value i is $P_i = N_i / N$. Set t as the threshold, and the gray level of the original image can be divided into two regions: background region $A = (0,1,\cdots,t)$ and target region $B = (t+1,t+2,\cdots,L-1)$. The probability of each region is:

$$P_A = \sum_{i=0}^{t} P_i \tag{9}$$

$$P_B = \sum_{i=t+1}^{L-1} P_i \tag{10}$$

The average grayscale value of each region is:

$$\omega_A = \sum_{i=0}^{t} i * \frac{P_i}{P_A} \tag{11}$$

$$\omega_B = \sum_{i=t+1}^{L-1} i * \frac{P_i}{P_B} \tag{12}$$

The average grayscale value of original image is:

$$\omega_0 = P_A \omega_A + P_B \omega_B + \sum_{i=0}^{L-1} i * P_i \tag{13}$$

Therefore, the inter-class variance of region A and B is:

$$\sigma^2 = P_A(\omega_A - \omega_0)^2 + P_B(\omega_B - \omega_0)^2 \tag{14}$$

The bigger variance σ^2, the greater difference between two gray level region. And the value T that maximizes the variance σ^2 is the optimal threshold:

<center>9</center>

$$\sigma^2 = \underset{0<t<L-1}{MAX}[P_A(\omega_A - \omega_0)^2 + P_B(\omega_B - \omega_0)^2], \qquad when \quad t = T \qquad (15)$$

The basic principle of the local adaptive threshold segmentation algorithm is as follows:

$$\begin{pmatrix} f(x-1,y-1) & f(x-1,y) & f(x-1,y+1) \\ f(x,y-1) & f(x,y) & f(x,y+1) \\ f(x+1,y-1) & f(x+1,y) & f(x+1,y+1) \end{pmatrix}$$

$$\begin{aligned} S = &f(x-1,y-1)+f(x-1,y)+f(x-1,y+1)+f(x,y-1)+f(x,y) \\ &+f(x,y+1)+f(x+1,y-1)+f(x+1,y)+f(x+1,y+1) \end{aligned} \qquad (16)$$

$$f(x,y) = \begin{cases} 0, & \dfrac{S}{9} < T \\ 1, & \dfrac{S}{9} \geq T \end{cases} \qquad (17)$$

As shown in Eq. (16) and Eq. (17), a preset $3*3$ pixels window is used to slide pixel by pixel in the original image until the entire image is traversed.

In the sub-region image that corresponding to each window, the sum values S of all pixel in the window is calculated. If $S/9$ is greater than or equal to the threshold value T, the pixel value in the middle of the window is set to 1. Otherwise, set the pixel value in the middle of the window to 0. 1 indicates the target and 0 indicates background. After threshold segmentation, the original VMI image and VFI image are changed to binary image, as shown in Fig.10.

（a） （b）

Fig.10. Threshold segmentation image: (a) VMI tear image; (b) VFI wear image

2.4. Feature extraction

The conveyor belt longitudinal tear or wear occurs during the operation of the conveyor belt, and the longitudinal tear or wear is continuous. After above image processing, we can find that the area of longitudinal tear or wear appears as continuous parallel lines. Therefore, the Hough line transformation [29] is used to extract the parallel lines as the detection feature of the conveyor belt, and the distance between parallel lines is calculated as the basis for identification.

2.4.1. Hough line transformation

Hough line transformation is applied to the binary image. When the conveyor belt longitudinal tear or wear occurs, a continuous straight line existing on VMI image and VFI image can be obtained. The steps of Hough line transformation are as follows:

(1) A line can be represented by two variables in the two-dimensional space:

a. In Cartesian coordinates: a line can be represented by parameter (m,b) slope and intercept;

b. In polar coordinates: a line can be represented by parameters (r,θ) radius and angle.

The expression of a straight line using polar coordinate is:

$$r = x*\cos\theta + y*\sin\theta \qquad (18)$$

(2) For the point (x_0, y_0), all lines passing through this point are defined as:

$$r_\theta = x_0*\cos\theta + y_0*\sin\theta \qquad (19)$$

means that each pair (r_θ, θ) represents a straight line passing through the point (x_0, y_0);

(3) For a given point (x_0, y_0), plot all the lines passing through it in the polar coordinates and get a sine curve;

(4) Repeat above operation for all points in the original image. If the curves that obtained from two different points intersect in the polar coordinate plane, it means that they pass the same straight line;

(5) Set threshold value, and count the number of curves corresponding to each intersection point in the image. If the number of curves intersecting one point exceeds the threshold value, then the parameter pair (r_θ, θ) represented by this intersection point is considered to be a straight line in the original image. The Hough line transformation results of the VMI tear image and the VFI wear image are shown in Fig.11.
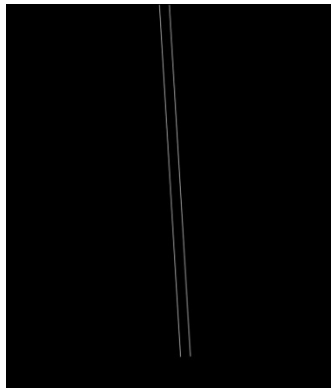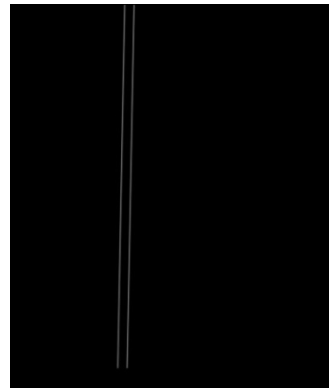
（a）   （b）

Fig.11. Hough line transformation results: (a) VMI tear images; (b) VFI wear images

2.4.2. Parallel lines distance detection

Thinning the parallel lines by using Hilditch's algorithm [30] after Hough line transformation. Then the distance between parallel lines is calculated to provide data basis for the subsequent conveyor belt status analysis. The calculation method of parallel lines distance is as follows:

(1) The equation of parallel lines that obtained by Hough line transformation is shown as following:

$$\begin{cases} Ax + By + C_1 = 0 \\ Ax + By + C_2 = 0 \end{cases} \tag{20}$$

(2) The distance between parallel lines is the distance from any point on one line to another line. If point $P(a,b)$ is on the line $Ax + By + C_1 = 0$, then $Aa + Bb = -C_1$;

(3) The distance from point $P(a,b)$ to line $Ax + By + C_2 = 0$ is:

$$d = \frac{|Aa + Bb + C_2|}{\sqrt{A^2 + B^2}} = \frac{|-C_1 + C_2|}{\sqrt{A^2 + B^2}} = \frac{|C_2 - C_1|}{\sqrt{A^2 + B^2}} \tag{21}$$

where d is the distance between parallel lines is:

2.5. Status analysis

According to the actual situation of the experiment and the industrial site conveyor belt, the width of crack is larger than the width of the scratch. For the VMI images, in order to distinguish cracks and scratches, thresholds t_1 and t_2 (pixel) are set. When the distance between parallel lines in the VMI image is greater than t_2, it is determined that there is a crack on the conveyor belt. When the distance is less than t_2 and greater than t_1, it is determined that there is a scratch on the conveyor belt. When the distance is less than t_1, it is determined that there is no scratch or crack on the conveyor belt. For the VFI images, in order to identify wear, threshold value T (pixel) is set. When the distance between parallel lines in the VFI image is greater than T, it is determined that the conveyor belt wear is occurring ,when the distance is less than T, it is determined that there is no wearing on the conveyor belt. The judgment formulas are as follows:

$$\begin{cases} d < t_1, & VMI = 0, No \text{ scratch or crack} \\ t_1 \le d < t_2, & VMI = 1, Conveyor \text{ belt has scratch} \\ d \ge t_2, & VMI = 2, Conveyor \text{ belt has crack} \end{cases} \tag{22}$$

$$\begin{cases} D<T, & VFI=0, Conveyor \text{ belt is not wearing} \\ D \ge T, & VFI=1, Conveyor \text{ belt is wearing} \end{cases} \tag{23}$$

where d is the distance between parallel lines in the VMI image, D is the distance between parallel lines in the VFI image. Combined with the analysis results of VMI images and VFI images, the status of conveyor belt can be determined, as shown in Table 1.

Table 1

Status analysis of conveyor belt

VMI	VFI	Status of conveyor belt	Operation
0	0	Conveyor belt normal	Normal running
0	1	Upper surface wearing	Danger alarm
1	0	Wear has happened but have not repaired	Warning alarm
1	1	Lower surface wearing	Danger alarm
2	0	Longitudinal tear has happened but have not repaired	Warning alarm
2	1	Longitudinal tearing	Stop conveyor

3. Experimental and analysis

In order to verify the proposed multispectral visual detection method, an experimental platform was set up in the laboratory. The experimental results show that the proposed method is effective and reliable. The experimental procedures, results and analysis are as follows:

3.1. Experimental procedures

The conveyor belt used in the experimental platform is a common steel cord conveyor belt for coal mine. The actual picture of the experimental platform is shown in Fig.12. The width of conveyor belt is 0.8m, total length is 23m, thickness is 15mm, and the maximum running speed is 4m/s. Two steel chisels were installed on the experimental platform. The steel chisels can rub against conveyor belt and then penetrate the conveyor belt to cause longitudinal tear. The installation method of the steel chisels is shown in the Fig.13. The pixels of visible light CCD, mid-infrared CCD and far infrared CCD are all 420×380. The experimental environment for image processing and analysis is a personal computer: the CPU is Inter Core E7500 2.93GHz, memory is 4GB, and the programming software is Microsoft Visual Studio (VS) with open source computer vision library (Open CV).
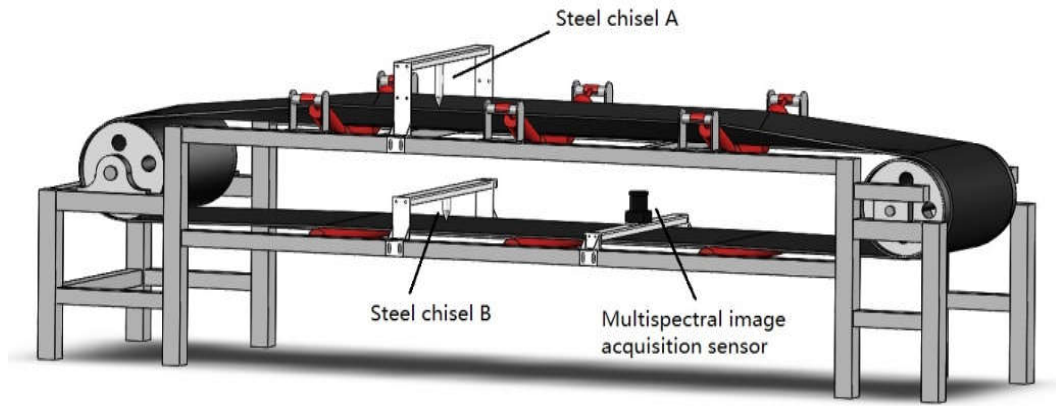

Fig.12. Experimental platform

Fig.13. Installation diagram of the steel chisels

All experiments were carried out in dark and dusty environment. The experiment was carried out six times, experiment 1-3 were the conveyor belt upper surface wear and then longitudinal tear, experiment 4-6 were the conveyor belt lower surface wear and then longitudinal tear. The specific experimental steps of conveyor belt upper surface wear and then longitudinal tear are as follows:

(1) Adjusted the steel chisel A to be pressed on the upper surface of the conveyor belt as far as possible;

(2) Started the belt conveyor and started image acquisition, the steel chisel A first rubbed against the conveyor belt and then penetrated the conveyor belt to cause longitudinal tear;

(3) Stopped the belt conveyor, adjusted the steel chisel A to leave away from conveyor belt. Then restart the belt conveyor to complete the conveyor belt image acquisition that has been worn and longitudinal torn.

The experimental steps of conveyor belt lower surface wear and then longitudinal tear are similar to the above steps except that the steel chisel B was adjusted to be pressed against the lower surface of the conveyor belt. The flowchart of multispectral visual detection method is shown in the Fig.14.
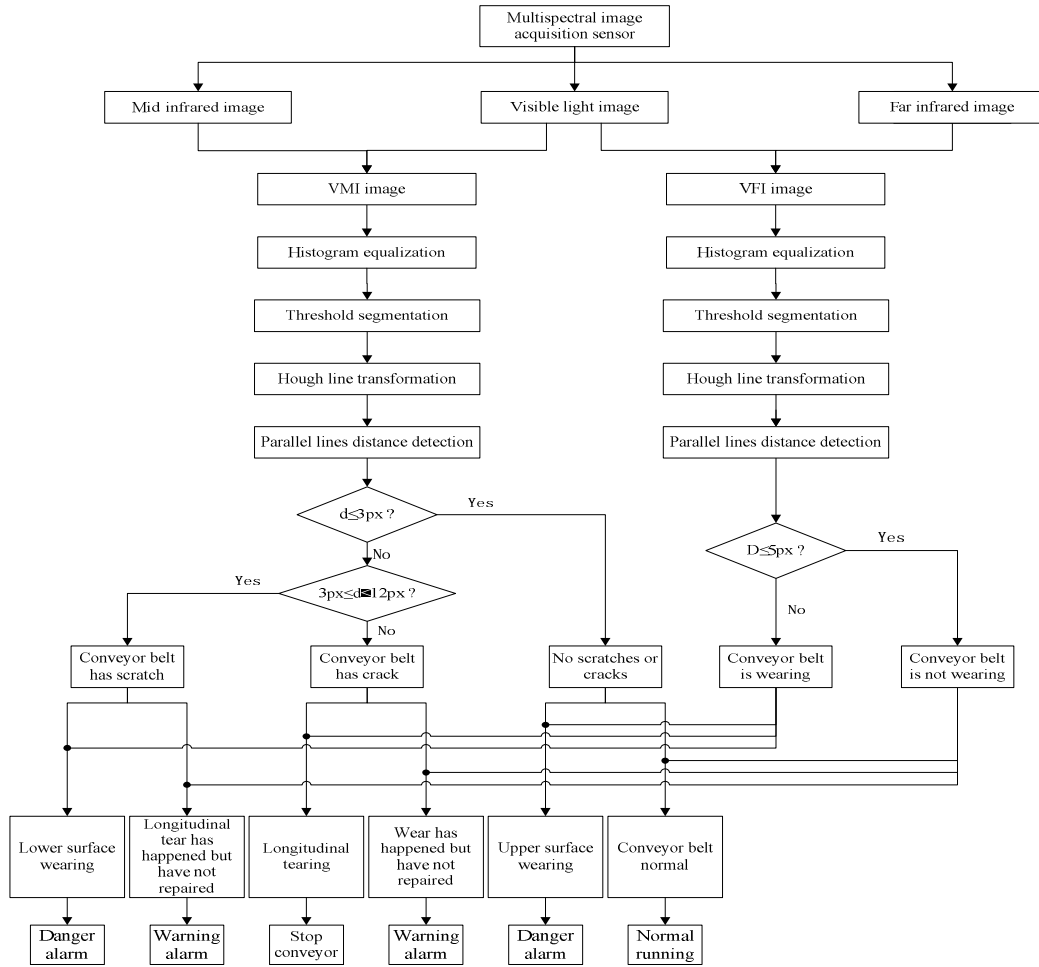
Fig.14. The flowchart of multispectral visual detection method

3.2. Experimental results and analysis

Experiment was carried out six times, and the number of each status image were shown in Table 2. Since the multispectral image acquisition sensor could not capture the upper surface image of the conveyor belt, the item of upper wear has happened was not listed in the Table 2. Experiment 1-3 were the conveyor belt upper surface wear and then longitudinal tear, there was no image about lower surface wearing or lower wear has happened but have not repaired. Experiment 4-6 were the conveyor belt lower surface wear and then longitudinal tear, there was no image about upper surface wearing. The minimum total number of image was 520 which in the experiment 1, the maximum total number of image was 717 which in experiment 4.

Table 2

Image statistics of multispectral visual detection method

Experiment	Conveyor belt normal	Upper surface wearing	Lower surface wearing	Longitudinal tearing	Lower wear has happened but have not repaired	Longitudinal tear has happened but have not repaired
1	125	133	0	120	0	142
2	154	111	0	128	0	132
3	119	156	0	117	0	124

15

4	131	0	145	143	153	145
5	115	0	123	135	142	139
6	142	0	142	119	143	125

According to the experimental images, the thresholds t_1 and t_2 for distinguishing cracks and scratches were set as $t_1 = 3px$ and $t_2 = 12px$ (pixel), and the threshold T for determining wear was set as $T = 5px$. The analysis results of the conveyor belt image were shown in Table 3, and the accuracy rate statistics were shown in Table 4. In experiment 1, the accuracy rate of longitudinal tearing recognition was 97.5%, and the total number that misidentification of lower surface wearing and lower wear has happened but have not repaired was 17 frames, accounting for 3.3% of the total number, and the average accuracy rate was 96.7%. In experiment 4, the accuracy rate of longitudinal tearing recognition was 96.5%, the total number that misidentification of upper surface wearing was 20 frames, accounting for 2.8% of the total number, and the average accuracy rate was 97.2%. In the six experiments, the highest recognition accuracy rate of longitudinal tearing was 97.5%, and the lowest recognition accuracy rate of longitudinal tearing was 96.5%, the highest average accuracy rate was 97.2%, and the lowest average accuracy rate was 96.1%. The experiments show that the multispectral visual detection method can be used to identify and classify all status of the conveyor belt. The average processing time of a single frame image was less than 30ms, which meets the requirement of online real-time detection for conveyor belt longitudinal tear.

Table 3

Analysis result of multispectral visual detection method

Experiment	Conveyor belt normal	Upper surface wearing	Lower surface wearing	Longitudinal tearing	Lower wear has happened but have not repaired	Longitudinal tear has happened but have not repaired
1	119	128	7	117	10	139
2	151	106	10	124	9	125
3	115	152	7	113	8	121
4	128	20	143	138	147	141
5	110	25	117	131	137	134
6	137	22	137	115	139	121

Table 4

Accuracy statistics of multispectral visual detection method

Experiment	Conveyor belt normal	Upper surface wearing	Lower surface wearing	Longitudinal tearing	Lower wear has happened but have not repaired	Longitudinal tear has happened but have not repaired	Average accuracy rate	Average processing time (ms)
1	95.2%	96.2%	—	97.5%	—	97.9%	96.7%	24.756
2	98.1%	95.5%	—	96.9%	—	94.7%	96.3%	28.931
3	96.6%	97.4%	—	96.6%	—	97.6%	97.1%	26.742
4	97.7%	—	98.6%	96.5%	96.1%	97.2%	97.2%	29.015
5	95.7%	—	95.1%	97.0%	96.5%	96.4%	96.1%	27.158
6	96.5%	—	96.5%	96.6%	97.2%	96.8%	96.7%	27.482

4. Conclusion

This paper proposed a multispectral visual detection method to achieve conveyor belt longitudinal tear and other status detection. A dedicated multispectral image acquisition sensor was used to capture visible light, mid-infrared and far infrared images. And then image fusion, processing and feature extraction were performed to determine the status of the conveyor belt. An experimental platform was built in the laboratory. The experimental results show that the proposed multispectral vision detection method not only can recognize the conveyor belt longitudinal tearing, but also can recognize the conveyor belt wearing, normal, the wear or tear has happened but have not repaired. The accuracy of longitudinal tear recognition is over 96.5%, and the average accuracy is over 96.1%, meeting real-time and reliability requirements. Future research will focus on the study of threshold settings for various conveyor belts to make the proposed detection method more widely applicable.

5. Conflicts of interest

The authors declare no conflict interest.

Acknowledgements

References

[1]   D. He, Y. Pang, G. Lodewijks, X. Liu, Healthy speed control of belt conveyors on conveying bulk materials, Powder Technol. 327 (2018) 408–419. doi:10.1016/j.powtec.2018.01.002.

[2]   T. Braun, A. Hennig, B.G. Lottermoser, The need for sustainable technology diffusion in mining: Achieving the use of belt conveyor systems in the German hard-rock quarrying industry, J. Sustain. Min. 16 (2017) 24–30. doi:10.1016/j.jsm.2017.06.003.

[3]   Y. Huang, W. Cheng, C. Tang, C. Wang, Study of multi-agent-based coal mine environmental monitoring system, Ecol. Indic. 51 (2015) 79–86. doi:10.1016/j.ecolind.2014.09.047.

[4]   J. Li, C. Miao, The conveyor belt longitudinal tear on-line detection based on improved SSR algorithm, Opt. - Int. J. Light Electron Opt. 127 (2016) 8002–8010. doi:10.1016/j.ijleo.2016.05.111.

[5]   Y. Pang, G. Lodewijks, A novel embedded conductive detection system for i[1] Y. Pang, G. Lodewijks, A novel embedded conductive detection system for intelligent conveyor belt monitoring, 2006 IEEE International Conference on Service Operations and Logistics, and Informatics, SO, 2006 IEEE Int. Conf. Serv. Oper. Logist. Informatics, SOLI 2006. (2006) 803–808. doi:10.1109/SOLI.2006.235556.

[6]   S.TANG, M.TONG，, B.WANG，, C.JIANG，, Z.TONG，, New Detection Method for Longitudinal T ear of Conveyor Belt in Coal Mine, Coal Mine Mach. (2013) 191–193. doi:10.13436/j.mkjx.2013.10.098.

[7]   V. Molnár, G. Fedorko, M. Andrejiová, A. Grinčová, M. Tomašková, Analysis of influence of

conveyor belt overhang and cranking on pipe conveyor operational characteristics, Meas. J. Int. Meas. Confed. 63 (2015) 168–175. doi:10.1016/j.measurement.2014.12.013.

[8]   R. Błażej, L. Jurdziak, T. Kozłowski, A. Kirjanów, The use of magnetic sensors in monitoring the condition of the core in steel cord conveyor belts – Tests of the measuring probe and the design of the DiagBelt system, Meas. J. Int. Meas. Confed. 123 (2018) 48–53. doi:10.1016/j.measurement.2018.03.051.

[9]   M. Leo, G. Medioni, M. Trivedi, T. Kanade, G.M. Farinella, Computer vision for assistive technologies, Comput. Vis. Image Underst. 154 (2017) 1–15. doi:10.1016/j.cviu.2016.09.001.

[10]   M. Soprana, A.C. Santomaso, P. Facco, Artificial vision system for the online characterization of the particle size distribution of bulk materials on conveyor belts, in: Comput. Aided Chem. Eng., Elsevier, 2018: pp. 1667–1672. doi:10.1016/B978-0-444-64235-6.50290-4.

[11]   Y. Yang, C. Miao, X. Li, X. Mei, On-line conveyor belts inspection based on machine vision, Optik (Stuttg). 125 (2014) 5803–5807. doi:10.1016/j.ijleo.2014.07.070.

[12]   G. Rosati, G. Boschetti, A. Biondi, A. Rossi, Real-time defect detection on highly reflective curved surfaces, Opt. Lasers Eng. 47 (2009) 379–384. doi:10.1016/j.optlaseng.2008.03.010.

[13]   L. Xianguo, S. Lifang, M. Zixu, Z. Can, J. Hangqi, Laser-based on-line machine vision detection for longitudinal rip of conveyor belt, Optik (Stuttg). 168 (2018) 360–369. doi:10.1016/j.ijleo.2018.04.053.

[14]   B. Yu, T. Qiao, H. Zhang, G. Yan, Dual band infrared detection method based on mid-infrared and long infrared vision for conveyor belts longitudinal tear, Meas. J. Int. Meas. Confed. 120 (2018) 140–149. doi:10.1016/j.measurement.2018.02.029.

[15]   T. Qiao, L. Chen, Y. Pang, G. Yan, C. Miao, Integrative binocular vision detection method based on infrared and visible light fusion for conveyor belts longitudinal tear, Measurement. 110 (2017) 192–201. doi:10.1016/j.measurement.2017.06.032.

[16]   F. Hakami, A. Pramanik, N. Ridgway, A.K. Basak, Developments of rubber material wear in conveyer belt system, Tribol. Int. 111 (2017) 148–158. doi:10.1016/j.triboint.2017.03.010.

[17]   G. Fedorko, V. Molnar, A. Grincova, M. Dovica, T. Toth, N. Husakova, V. Taraba, M. Kelemen, Failure analysis of irreversible changes in the construction of rubber-textile conveyor belt damaged by sharp-edge material impact, Eng. Fail. Anal. 39 (2014) 135–148. doi:10.1016/j.engfailanal.2014.01.022.

[18]   G. Fedorko, V. Molnár, S. Honus, M. Beluško, M. Tomašková, Influence of selected characteristics on failures of the conveyor belt cover layer material, Eng. Fail. Anal. 94 (2018) 145–156. doi:10.1016/j.engfailanal.2018.07.034.

[19]   M. Andrejiova, A. Grincova, D. Marasova, Measurement and simulation of impact wear damage to industrial conveyor belts, Wear. 368–369 (2016) 400–407. doi:10.1016/j.wear.2016.10.010.

[20]   B. Sun, N. Yuan, C. Cao, J.Y. Hardeberg, Design of four-band multispectral imaging system with one single-sensor, Futur. Gener. Comput. Syst. 86 (2018) 670–679. doi:10.1016/j.future.2018.04.056.

[21]   N. Aishwarya, C. Bennila Thangammal, Visible and infrared image fusion using DTCWT and adaptive combined clustered dictionary, Infrared Phys. Technol. 93 (2018) 300–309. doi:10.1016/j.infrared.2018.08.013.

[22]   Y. Liu, X. Chen, Z. Wang, Z.J. Wang, R.K. Ward, X. Wang, Deep learning for pixel-level image fusion: Recent advances and future prospects, Inf. Fusion. 42 (2018) 158–173. doi:10.1016/j.inffus.2017.10.007.

[23]   R. Vijayarajan, S. Muttan, Discrete wavelet transform based principal component averaging fusion for medical images, AEU - Int. J. Electron. Commun. 69 (2015) 896–902. doi:10.1016/j.aeue.2015.02.007.

[24]   F. Meng, M. Song, B. Guo, R. Shi, D. Shan, Image fusion based on object region detection and Non-Subsampled Contourlet Transform, Comput. Electr. Eng. 62 (2017) 375–383. doi:10.1016/j.compeleceng.2016.09.019.

[25]   K. Verma, B. Kumar Singh, A.S. Thokec, An enhancement in adaptive median filter for edge preservation, Procedia Comput. Sci. 48 (2015) 29–36. doi:10.1016/j.procs.2015.04.106.

[26]   Z. Fan, D. Bi, W. Ding, Infrared image enhancement with learned features, Infrared Phys. Technol. 86 (2017) 44–51. doi:10.1016/j.infrared.2017.08.015.

[27]   Y. Wang, Z. Pan, Image contrast enhancement using adjacent-blocks-based modification for local histogram equalization, Infrared Phys. Technol. 86 (2017) 59–65. doi:10.1016/j.infrared.2017.08.005.

[28]   I. Lee, X. Du, B. Anthony, Hair segmentation using adaptive threshold from edge and branch length measures, Comput. Biol. Med. 89 (2017) 314–324. doi:10.1016/j.compbiomed.2017.08.020.

[29]   P. Mukhopadhyay, B.B. Chaudhuri, A survey of Hough Transform, Pattern Recognit. 48 (2015) 993–1010. doi:10.1016/j.patcog.2014.08.027.

[30]   M. Naseri, S. Heidari, R. Gheibi, L.H. Gong, M. Ahmadzadeh Rajii, A. Sadri, A novel quantum binary images thinning algorithm: A quantum version of the Hilditch's algorithm, Optik (Stuttg). 131 (2017) 678–686. doi:10.1016/j.ijleo.2016.11.124.